

Spectroscopy of capacitively coupled Josephson-junction qubits

Philip R. Johnson, Frederick W. Strauch, Alex J. Dragt, Roberto C. Ramos, C. J. Lobb, J. R. Anderson, and F. C. Wellstood

Department of Physics, University of Maryland, College Park, Maryland 20742-4111
(Dated: October 23, 2018)

We show that two capacitively-coupled Josephson junctions, in the quantum limit, form a simple coupled qubit system with effective coupling controlled by the junction bias currents. We compute numerically the energy levels and wave functions for the system, and show how these may be tuned to make optimal qubits. The dependence of the energy levels on the parameters can be measured spectroscopically, providing an important experimental test for the presence of entangled multiqubit states in Josephson-junction based circuits.

PACS numbers: 74.50.+r, 03.67.Lx, 85.25.Cp

Keywords: Qubit, quantum computing, superconductivity, Josephson junction.

Ramos *et al.* have proposed that electrically well-isolated Josephson junctions can be used as qubits [1]. Two recent experiments using different isolation schemes have reported Rabi oscillations in single junctions [2], demonstrating the existence of macroscopic quantum coherence. While longer coherence times are desirable, these experiments show that single Josephson junctions are strong candidates for solid-state qubits; several Josephson-based types have been proposed [3].

One of the next major steps towards building a Josephson-junction based quantum computer will be the observation of quantum properties of coupled macroscopic qubits. A simple scheme for making coupled qubits, junctions connected by capacitors, has recently been proposed by Blais *et al.* [4] and Ramos *et al.* [5]. This scheme is illustrated for the two-qubit case in Fig. 1(a).

In this paper, we focus on the immediately accessible fundamental experiments—spectroscopic measurements of macroscopically entangled quantum states—that are possible with this system. We calculate, using highly accurate numerical methods, the energy levels and metastable wave functions for the circuit of Fig. 1(a) in terms of the junction parameters, bias currents, and coupling capac-

itance. Our numerical analysis demonstrates that the system can be tuned to create appropriately spaced energy levels and coupled states. The features that we discuss can both guide the experimental effort of observing multiqubit quantum states and provide help in optimizing the design of qubits and gates. But we emphatically stress that experimental observation of these macroscopic entangled quantum states will be an important achievement in its own right, and will provide strong support for the validity of macroscopic quantum mechanics and the existence of macroscopic entanglement [6]. Spectroscopic observation of these states should be possible by using standard single-junction experimental techniques [5, 7].

The Hamiltonian for an ideal single current-biased Josephson junction, with critical current I_c and junction capacitance C_J , is

$$H(\gamma, p) = (4E_C \hbar^{-2}) p^2 - E_J (\cos \gamma + J\gamma), \quad (1)$$

where γ is the gauge-invariant phase difference across the junction, $J = I/I_c$, I is the (tunable) bias current, $E_J = (\Phi_0 I_c / 2\pi)$ is the Josephson energy, $E_C = e^2 / 2C_J$ is the charging energy, and $\Phi_0 = h/2e$ is the flux quantum. The canonical momentum is $p = (\Phi_0 / 2\pi)^2 C_J \dot{\gamma} = \hbar Q / 2e$, where Q is the charge on the junction. The ratio E_J / E_C determines whether the system is in a phase, charge, or intermediate regime. The qubits explored in this paper have $E_J \gg E_C$ and hence are in the phase regime.

The equations of motion for a single current-biased junction are equivalent to those for a particle in the tilted washboard potential shown in Fig. 1(b). Classically, for $J < 1$ there are stable minima about which the phase can oscillate with the characteristic plasma frequency $\omega_p(J) = \sqrt{2\pi I_c / \Phi_0 C_J} (1 - J^2)^{1/4}$ [8]. Quantum mechanically, the system exhibits localized metastable states in each well that can tunnel out into the running (finite-voltage) state. The effective barrier height $\Delta U_{\text{barrier}}$ [see Fig. 1(b)] for a single junction in units of

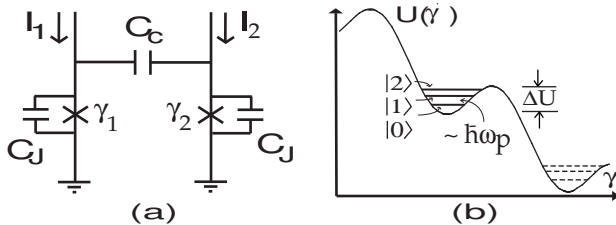


FIG. 1: (a) (left) Circuit diagram for two idealized capacitively coupled Josephson junctions. (b) (right) The tilted washboard potential for a single current-biased Josephson junction with three metastable quantum states.

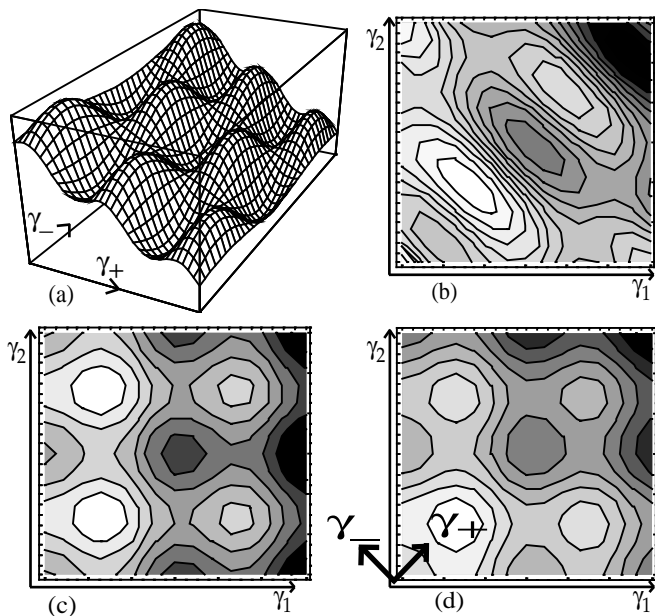


FIG. 2: (a) Potential V' with strong coupling ($\zeta = 0.8$) and $J_1 = J_2$. The coupling induces a squeezing in the γ_+ direction, relative to the γ_- direction. (b) V' contours with $\zeta = 0.8$ and $J_1 \neq J_2$, around the vicinity of one well. The symmetry of V' shows that, despite detuned bias currents, γ_+ and γ_- are approximately the normal modes. (c) V' with small coupling ($\zeta = 0.01$) and $J_1 \neq J_2$ showing (by symmetry) that γ_1 and γ_2 are approximate normal modes. (d) V' with $\zeta = 0.01$ and $J_1 = J_2$ showing that γ_+ and γ_- are normal modes.

$\hbar\omega_p(J)$, assuming $J \lesssim 1$, is related to N_s by

$$N_s \simeq \frac{\Delta U_{\text{barrier}}}{\hbar\omega_p(J)} = \frac{2^{3/4}}{3} \left(\frac{E_J}{E_C} \right)^{1/2} (1 - J)^{5/4}. \quad (2)$$

Here, N_s is the approximate number of metastable bound states for a single isolated junction [8]. Our analysis explores the relevant regime for quantum computing where N_s is small and the nonlinearity of the Hamiltonian is important.

By adjusting the bias current it is possible to tune the barrier height to obtain, for example, three metastable energy levels $E_0 < E_1 < E_2$ with the two lowest states forming the basis $|0\rangle, |1\rangle$ of a qubit. State $|2\rangle$ has the highest escape rate due to tunneling and can therefore act as an auxiliary readout state, where readout is achieved by microwave pumping at a frequency $\omega_{12} = (E_2 - E_1)/\hbar$. Detection of a voltage across the junction implies that the system was previously in the state $|1\rangle$ and has entered the running state.

The Hamiltonian for the coupled two-junction circuit shown in Fig. 1(a) is

$$H = \frac{4E_C}{(1 + \zeta)\hbar^2} (p_1^2 + p_2^2 + 2\zeta p_1 p_2) - E_J (\cos \gamma_1 + \cos \gamma_2 + J_1 \gamma_1 + J_2 \gamma_2), \quad (3)$$

where $\zeta = C_C/(C_C + C_J)$ is the dimensionless coupling parameter, C_C is the coupling capacitance, and $J_{1,2}$ are the normalized bias currents of junctions 1 and 2, respectively. The canonical momenta, $p_{1,2} = (C_C + C_J) (\Phi_0/2\pi)^2 (\dot{\gamma}_{1,2} - \zeta \dot{\gamma}_{2,1})$, are proportional to the charges on each junction plus the charge on the coupling capacitor plate adjacent to it [4, 5].

By making a canonical change of variables, defined by

$$\gamma_{\pm} = (\gamma_1 \pm \gamma_2) / \sqrt{2(1 \pm \zeta)}, \quad (4)$$

$$p_{\pm} = \sqrt{2(1 \pm \zeta)} (p_1 \pm p_2), \quad (5)$$

we find the transformed Hamiltonian

$$H'(p_+, p_-, \gamma_+, \gamma_-) = \frac{4E_C}{(1 + \zeta)\hbar^2} (p_+^2 + p_-^2) + V'(\gamma_+, \gamma_-). \quad (6)$$

Here, the momentum coupling term $2\zeta p_1 p_2$ in the original Hamiltonian is shifted to coupling in the new potential energy $V' = V'(\gamma_+, \gamma_-)$. Figures 2(a,b) illustrate how the coupling induces a squeezing of V' along the γ_+ direction; a strong coupling of $\zeta = 0.8$ has been chosen to accentuate this behavior.

We gain further insight into the coupling of the junction states by looking at the normal modes for small oscillations. For small coupling and detuned bias currents (J_1 far from J_2) the normal modes are approximately γ_1 and γ_2 , i.e., the junctions are effectively decoupled. This effect is shown in Fig. 2(c) by the approximate symmetry of V' with respect to reflections about the γ_1 and γ_2 axes. When $J_1 = J_2$ the normal modes become γ_+ and γ_- , and we therefore expect the coupled junction states to be entangled symmetric and antisymmetric combinations of the single junction states. This can be seen in Fig. 2(d), where V' is symmetric with respect to reflections about the γ_+ and γ_- axes. Figure 2(b) shows V' for $\zeta = 0.8$ and unequal bias currents; despite detuning the large ζ prevents the junctions from decoupling and γ_+ and γ_- effectively remain as normal modes.

The challenging demands of quantum computing require an accurate and precise quantitative description of the states going beyond simple perturbation theory. To achieve this, we have computed the states and energy levels numerically using a nonperturbative fast Fourier transform split-operator method [9] applied to the full nonlinear Hamiltonian in Eq. (3). Our implementation computes the wave functions on a lattice using a fourth-order integration of the imaginary-time evolution operator $\exp(-\hat{H}\tau)$. While this method is relatively slow, its results for a subset of system parameters confirm that the much faster complex scaling method [10] applied to the cubic approximation of the full potential [6] is accurate to at least 0.1%. The faster complex scaling method then allows us to compute energy levels for a wide range of system parameters. A further important property of both these numerical methods is that they are well suited to

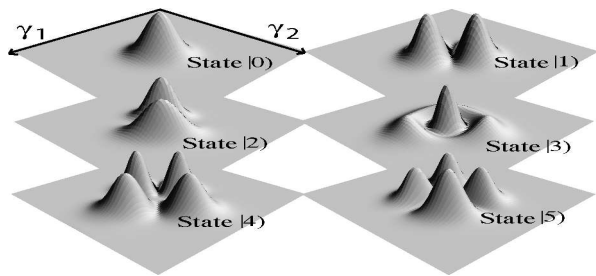


FIG. 3: The modulus squared of the probability amplitude of the first six quasistationary wave functions for capacitively coupled current-biased Josephson junctions with coupling of $\zeta = 0.01$ and normalized bias currents of $J_1 = J_2 = 0.98693$.

finding metastable states in potentials that allow tunneling, particularly in more than one dimension, where other methods fail. The computed quantum states have been further verified by time evolving them on a lattice using real time split-operator methods. This has confirmed dynamically that these states are truly quasistationary and thus accurately determined; where applicable, agreement has also been found with higher-order WKB analysis.

In Fig. 3 we show, for example, the numerically computed wave functions for identical junctions with capacitances $C_J = 4.3$ pF and critical currents $I_c = 13.3$ μ A. Junctions with these physical characteristics are readily fabricated and of physical interest. Figure 3 shows the modulus squared of the wavefunctions of the first six quasistationary states for the coupling strength $\zeta = 0.01$, and with bias currents $J_1 = J_2 = 0.98693$ such that isolated junctions would have approximately three quasistationary states ($N_s \simeq 3$). These large bias currents make the nonlinearities of the potential pronounced, and the states deviate significantly from coupled harmonic-oscillator states. The states $|n\rangle$ in Fig. 3 are ordered by energy E_n ; a rounded bracket has been used to distinguish the coupled two-junction states $|n\rangle$ from single-junction states $|n\rangle$. The second and third states expressed in terms of single-junction direct product states are $|1\rangle \cong (|01\rangle - |10\rangle)/\sqrt{2}$ and $|2\rangle \cong (|01\rangle + |10\rangle)/\sqrt{2}$, whereas the higher-energy states are more complicated superpositions that depend upon the bias currents and coupling. The ordering of the states in Fig. 3 may be understood by looking at the potentials shown in Fig. 2(a,b); wave functions extended in the γ_+ direction have higher energy because of the coupling induced effective squeezing in the γ_+ direction, relative to the γ_- direction. Observe that because the (γ_1, γ_2) configuration space variables are the collective degrees of freedom of distinct junctions, the wave functions represent macroscopic nonlocally correlated (and hence entangled) states.

For designing qubits out of coupled junctions we need to know how the energy levels depend on coupling and bias current. Figure 4 shows the effects of varying the

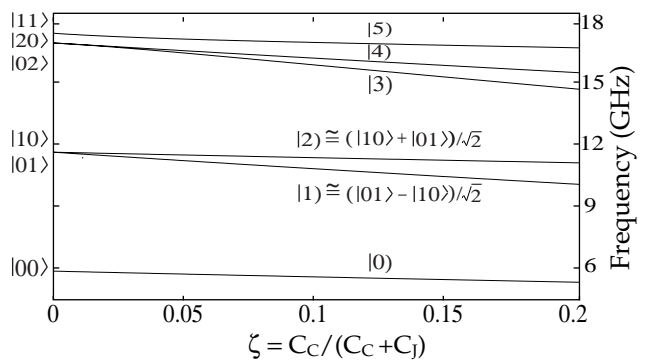


FIG. 4: Frequencies versus coupling strength for equal bias currents $J_1 = J_2 = 0.98693$, $I_C = 13.3$ μ A, and $C_J = 4.3$ pF.

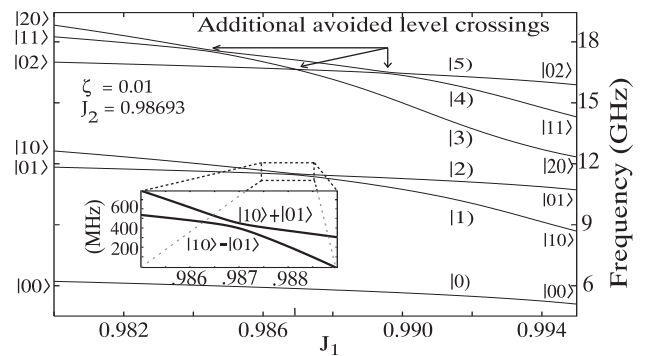


FIG. 5: Frequencies of the first six states versus bias current J_1 with $J_2 = 0.98693$ fixed and a coupling strength of $\zeta = 0.01$, $I_C = 13.3$ μ A, and $C_J = 4.3$ pF.

coupling strength in the range $0 < \zeta < 0.2$ on the first six energy levels with $J_1 = J_2 = 0.98693$. The plasma frequency of each single junction when $\zeta = 0$ is $\omega_p(J_1 = J_2)/2\pi = 6.2037$ GHz. The states are labeled at the left of Fig. 4 for zero coupling, where the product representation $|nm\rangle = |n\rangle \otimes |m\rangle$ is appropriate. For zero coupling the nonlinearity of the potential has broken the degeneracy between $|5\rangle = |11\rangle$ and the pair ($|3\rangle = |02\rangle, |4\rangle = |20\rangle$).

In real experiments, the coupling strength ζ will typically be fixed by the circuit design, and can only be varied by making a completely new sample. By contrast, the bias currents through each junction are easily varied, and allow manipulation of the entangled states shown in Fig. 3. Figure 5 shows how the energy levels change for $\zeta = 0.01$ and $J_2 = 0.98693$ fixed, while J_1 is varied around J_2 . There are prominent avoided level crossings indicated in the figure for both on-tune ($J_1 = J_2$) and off-tune ($J_1 \neq J_2$) bias currents. The predicted gap for the $|1\rangle, |2\rangle$ on-tune splitting at $J_1 = 0.98693$ is 57 MHz for $I_C = 13.3$ μ A and $C_J = 4.3$ pF. The predicted gap for the first off-tune splitting between states $|4\rangle$ and $|5\rangle$ at $J_1 = 0.98444$ is 80 MHz, and for the second off-tune

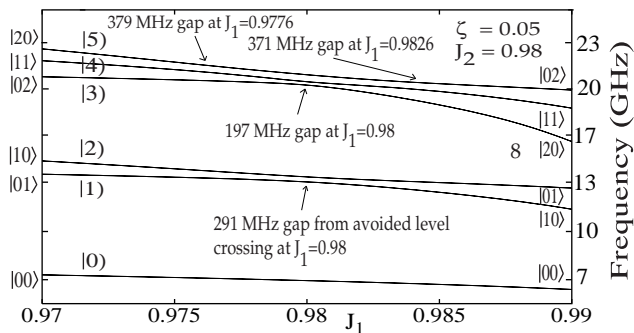


FIG. 6: Frequencies versus bias current J_1 with $J_2 = 0.98$ fixed and a coupling strength of $\zeta = 0.05$, $I_C = 13.3 \mu\text{A}$, and $C_J = 4.3 \text{ pF}$.

splitting at $J_1 = 0.98962$ the gap is 72 MHz. The predicted gap for the on-tune $|3\rangle, |4\rangle$ splitting of 4 MHz is much smaller than the others because it is a second-order avoided crossing in perturbation theory. Figure 6 shows the energy levels for the same junction parameters but with $\zeta = 0.05$ and $J_2 = 0.98$ ($N_s \simeq 5$).

We have labeled the states in Figs. 5 and 6 at the far left and right—when the currents are detuned and hence the states are effectively uncoupled—as product states. This labeling is only strictly correct when $\zeta = 0$. The mixing that occurs between states when the bias currents are brought into tune is indicated for the states $|1\rangle$ and $|2\rangle$ in Figs. 4 and 5. A swaplike gate operation can be constructed by exploiting this mixing [4].

Experimental data similar to Figs. 5 and 6 would be important first evidence for the existence of macroscopic entangled states like those shown in Fig. 3. A typical experiment to probe the energy levels in Figs. 4–6 would proceed by preparing the system in the ground state $|0\rangle$ by cooling well below $T \simeq E_{01}/k \simeq 300 \text{ mK}$, where $E_{nm} = (E_n - E_m)$, and $E_n = E_n(J_i, \zeta)$ are the coupled-junction energies whose dependence on bias current and coupling we have shown in Figs. 4–6. Varying the bias current J_1 (with J_2 fixed) while simultaneously injecting microwaves at a frequency $\bar{\omega}$ should lead to an enhancement in the tunneling from the zero-voltage state to the finite-voltage running state of the system when $\bar{\omega} = E_{nm}(J_1)/\hbar$. This enhancement produces a corresponding peak in escape rate measurements [5, 7]. By varying $\bar{\omega}$ and J_1 for the coupled junctions, we may map out the energy levels for comparison with Figs. 5 and 6.

Experimentally, the expected energy gap between the avoided levels can be resolved if both the quality factor Q and coupling ζ of the system are reasonably large. For example, with the typical junction parameters assumed here, and with $\zeta = 0.01$, the predicted gap for the $|1\rangle, |2\rangle$ splitting of 57 MHz can easily be resolved with a Q of 200 [5]. Furthermore, one can reasonably track the bending

of the resonant escape peaks near the avoided crossings within the span of a typical experimental current window of about 30 nA [5]. These splittings can be made even easier to detect by increasing the coupling capacitance (see Fig. 6), though large coupling may inhibit efficient quantum gates.

In conclusion, we have presented predictions for fundamental experiments that probe macroscopic entangled states by the relatively simple scheme of doing spectroscopy on coupled junctions while varying external bias currents. The energy levels of these entangled states should be readily observable using the same experimental techniques that have allowed spectroscopy of single junctions. The numerical methods we have used are powerful tools for mapping out the metastable states of nonlinear, many-level coupled systems, and allow us to explore a wide range of junction parameters and couplings. This kind of detailed study will be necessary for the design of realistic coupled qubits.

We would like to thank Andrew J. Berkley, Huizhong Xu, and Mark A. Gubrud for helpful discussions. This work was supported in part by the U.S. Department of Defense and the State of Maryland, through the Center for Superconductivity Research.

-
- [1] R. Ramos *et al.*, IEEE Trans. Appl. Supercond. **11**, 998 (2001).
 - [2] Y. Yu *et al.*, Science **296**, 889 (2002); J. M. Martinis *et al.*, Phys. Rev. Lett. **89**, 117901 (2002).
 - [3] S. Han, R. Rouse, and J. E. Lukens, Phys. Rev. Lett. **76**, 3404 (1996); M. F. Bocko, A. M. Herr, and M. J. Feldman, IEEE Trans. Appl. Supercond. **7**, 3638 (1997); J. E. Mooij *et al.*, Science **285**, 1036 (1999); C. H. van der Wal *et al.*, *ibid.* **290**, 773 (2000); J. R. Friedman *et al.*, Nature (London) **406**, 43 (2000); Y. Makhlin, G. Schön, and A. Shnirman, Rev. Mod. Phys. **73**, 357 (2001); D. Vion *et al.*, Science **296**, 886 (2002).
 - [4] A. Blais, A. Maassen van den Brink, and A. M. Zagoskin, condmat/0207112.
 - [5] R. C. Ramos *et al.*, IEEE Trans. Appl. Supercond. (to be published) (2002).
 - [6] A. J. Leggett, in *Chance and Matter*, edited by J. Souletie, J. Vannimenus, and R. Stora (Elsevier, Amsterdam, 1987), p. 395.
 - [7] J. M. Martinis, M. H. Devoret, and J. Clarke, Phys. Rev. Lett. **55**, 1543 (1985); Phys. Rev. B **35**, 4682 (1987).
 - [8] T. A. Fulton and L. N. Dunkleberger, Phys. Rev. B **9**, 4760 (1974).
 - [9] M. D. Feit, J. A. Fleck, Jr., and A. Steiger, J. Comput. Phys. **47**, 412 (1982); J. E. Bayfield, *Quantum Evolution* (Wiley, New York, 1999).
 - [10] R. Yaris *et al.*, Phys. Rev. A **18**, 1816 (1978); E. Caliceti, S. Graffi, and M. Maioli, Commun. Math. Phys. **75**, 51 (1980).